Materials Today Bio 31 (2025) 101637

Contents lists available at ScienceDirect

Materials Today Bio

journal homepage: www.journals.elsevier.com/materials-today-bio

An anti-inflammatory and anti-fibrotic Janus hydrogel for preventing postoperative peritoneal adhesion

Zhengjun Li [a,1], Lili Yang [a,b,1], Qi Jin [c], Wen Li [a,d], Yue Li [a,e], Yan Zheng [f], Mei Dong [a,e,**], Yaoyao Bian [a,d,g,*]

[a] Jiangsu Provincial Engineering Research Center of TCM External Medication Development and Application, Nanjing University of Chinese Medicine, Nanjing, 210023, China
[b] Jingwen Library, Nanjing University of Chinese Medicine, Nanjing, 210023, China
[c] Department of Polymer Science and Engineering, State Key Laboratory of Coordination Chemistry, Key Laboratory of High-Performance Polymer Material and Technology, MOE, School of Chemistry and Chemical Engineering, Nanjing University, Nanjing, Jiangsu, 210023, China
[d] School of Health Preservation and Rehabilitation, Nanjing University of Chinese Medicine, Nanjing, 210023, China
[e] School of Pharmacy, Nanjing University of Chinese Medicine, Nanjing, 210023, China
[f] Department of Polymer Science and Engineering, College of Materials Science and Engineering, Nanjing Tech University, Nanjing, Jiangsu, 211816, China
[g] TCM Rehabilitation Center, Jiangsu Second Chinese Medicine Hospital, Nanjing, 210023, China

ARTICLE INFO

Keywords:
Postoperative peritoneal adhesion
Janus hydrogel
Anti-inflammation
Anti-fibrosis
Collagen deposition

ABSTRACT

Postoperative peritoneal adhesion (PPA) is pathological tissue hyperplasia between surgical wounds and nearby organs. Currently, traditional double-sided bioadhesives are limited in preventing PPA due to the indiscriminate adhesive properties and the poor interaction with wet tissues. Herein, we developed a Janus hydrogel, named PAA-Cos, by using the polycationic carbohydrate polymer of chitooligosaccharide (Cos) and the polyanionic polymer of polyacrylic acid (PAA). The adhesive layer of Janus hydrogels could adhere to wet tissue tightly due to surfaces composed of carboxyls, and the positively charged biomaterial (Cos) neutralized carboxyls on one side of PAA hydrogel to form Janus hydrogels. Moreover, PAA-Cos can further load with ligustrazine hydrochloride (Ligu), a pharmaceutical compound with anti-inflammatory and anti-fibrotic effects, finally obtaining PAA-Cos@Ligu. After the application of PAA-Cos@Ligu on the surgical trauma, the bottom surface can adhere to wet tissues robustly to restore the wound, while the top surface acts as a physical barrier with antiadhesive effects to avoid PPA. PAA-Cos@Ligu also exhibited anti-inflammatory effects by promoting M2 macrophage polarization, inhibiting the myofibroblast-like differentiation of peritoneal mesothelial cells, and blocking the TGF-β/Smad2/3 signaling pathway to hinder collagen deposition. Our findings suggest that PAA-Cos@Ligu has great potential as an anti-adhesion candidate with biocompatibility and ease of preparation.

1. Introduction

Postoperative peritoneal adhesion (PPA) is characterized by pathological hyperplasia between wound sites and adjacent organs or tissues after surgical trauma [1]. The adhesion can be classified into membranous adhesion, vascular adhesion, adhesive adhesion, and scarred adhesion depending on the different compositions of these fibrous connections and the specific factors that contribute to its development [2]. Peritoneal adhesion occurs in a variety of postoperative diseases, such as parastomal hernia [3,4], and abdominoplasty [5]. PPA typically leads to a range of complications, such as chronic pain, female infertility, intestinal obstruction, and fistulas [6]. Because of the specific histological features of the peritoneal membrane and the polyorganic characteristics of the peritoneal cavity, up to 90 % of patients who underwent abdominal surgery experienced abdominal adhesions [7] and the recurrence rate of adhesion was as high as 80 % [8]. Meanwhile, nearly 35 % of Scottish patients were readmitted to hospital due to directly or indirectly adhesion-associated complications according to the retrospective cohort report [9,10]. As reported, the annual costs of adhesiolysis, a common surgical therapy for PPA, in the United States

* Corresponding author. School of Health Preservation and Rehabilitation, Nanjing University of Chinese Medicine, Nanjing, Jiangsu 210023, China.
** Corresponding author. School of Pharmacy, Nanjing University of Chinese Medicine, Nanjing, Jiangsu, 210023, China.
E-mail addresses: meidong707@njucm.edu.cn (M. Dong), bian@njucm.edu.cn (Y. Bian).
[1] ZJL and LLY contributed equally to this work.

https://doi.org/10.1016/j.mtbio.2025.101637
Received 13 December 2024; Received in revised form 23 February 2025; Accepted 3 March 2025
Available online 5 March 2025

were as high as $2.1 billion [11]. and the hospitalization costs for adhesion-associated small bowel obstruction reached up to €16, 305 in the Netherlands [12]. The costs of the second operation and adhesion-related complications not only bring a huge economic burden on individuals and families but also the public health system.

PPA is usually caused by peritoneal injury, initiated by an inflammatory reaction, and exacerbated by local repair. This pathophysiological process is rapid, cascaded, and complex [13]. Peritoneal mesothelial cells (PMCs) are primary barriers to the abdominal cavity, which is an essential cellular origin of adhesion, which could further cause the proliferation of myofibroblasts through epithelial-mesenchymal transition during peritoneal fibrosis [14]. Myofibroblasts are regarded as the key mediators of fibrosis during peritoneal adhesion formation, which can synthesize and secret excessive collagen and extracellular matrix, and play crucial roles in the fibrotic process [15]. Regardless of the significance of mesothelial cells in adhesion formation, polarization of macrophage is also recognized as a precursor of adhesion initiation [16], and is widely involved in inflammatory reactions [2]. It is well known that macrophages can be polarized into classically activated M1 macrophages and alternative proliferation-activated M2 macrophages. In the early inflammatory stage, M2 macrophages can release transforming growth factor-β (TGF-β) or respond to TGF-β signals to maintain immune homeostasis and promote tissue repair [17]. During the mid to late stages of inflammation, excessive TGF-β signal transduction may induce the myofibroblastic transition of PMCs, leading to ECM deposition, which in turn results in fibrosis and ultimately causes abdominal adhesion. Thus, maintaining the homeostasis of the immunoinflammatory environment and blocking the molecular processes that trigger the activation of mesothelial cells into myofibroblasts may provide a potential strategy to mitigate the excessive production of collagen and attenuate the development of adhesion.

In previous studies, a bioactive compound extracted from the root of *Ligusticum Chuanxiong hort* (*Umbelliferae*), exhibited beneficial effects in preventing adhesion formation both in *vivo* and in *vitro* [18–20]. Ligustrazine hydrochloride (Ligu) is a pharmaceutical compound that originates from the modification of ligustrazine, and it has been extensively utilized in clinics for its low toxicity and wide therapeutic effects. Yet, the disadvantages of Ligu with a short biological half-life, rapid metabolism, shorter retention time, and uneven distribution on mucosal surfaces limit its application in the PPA [21]. To better play the therapeutic effect of Ligu, a new delivery strategy should be developed to improve the druggability of Ligu.

In addition to drug therapies, physical barriers have been applied to clinical therapy for patients with PPA [6]. Fortunately, the Food and Drug Administration (FDA) has authorized the application of physical barriers, namely Seprafilm® and Interceed® [22]. Despite their extensive use in clinics, solid film products such as Interceed and Seprafilm are still far from ideal [23]. Hence, promising biomaterials used as physical barriers to prohibit PPA should have the following properties, including good biocompatibility, ease of preparation, and topical application [22]. Physical barriers formed by hydrogels arouse interest because of their longer retention time compared to direct application of drug solutions [24,25]. Further Janus hydrogels with different properties and distinct functions on its two sides are gradually used for the treatment of PPA [26]. Simultaneously, it has been reported that hydrogels composed of lightly crosslinked polyacrylic acid (PAA) can adhere to wet tissue tightly, which was based on the hydrogen bonding interaction between the carboxyl groups and wet tissue [27]. Due to all surfaces of hydrogels composed of PAA containing carboxyls, it is necessary to combine a positively charged biomaterial to neutralize carboxyls on one side to form Janus hydrogels. Chitosan, as a natural cationic polysaccharide with excellent biocompatibility, is composed of N-glucosamine and N-acetyl-glucosamine units [28,29]. However, the poor solubility in an aqueous solution restricts the application of chitosan to interact with PAA to form Janus hydrogels. Chitooligosaccharide (Cos), a degradation product of Chitosan, possessed good solubility [30,31] which could be selected to neutralize the carboxyls of PAA for preparing Janus hydrogels with one side without viscosity. Therefore, it is hypothesized that Janus hydrogels, featuring an adhesive hydrogel layer due to the presence of free carboxyl groups in PAA, and an anti-adhesive hydrogel layer resulting from the neutralization of these carboxyl groups with Cos, may exhibit promising therapeutic effects in preventing postoperative peritoneal adhesion formation.

In this study, we report a Janus hydrogel, which features an adhesive layer on its bottom surface and an anti-adhesive layer on its top surface, prepared using a one-step method via random polymerization with acrylic acid (AA) monomers. The Janus hydrogel could be further loaded with Ligu, a pharmaceutical compound with modulating homeostasis of macrophage polarization and anti-fibrosis, finally obtaining PAA-Cos@Ligu for preventing PPA, as shown in Fig. 1A. The Janus hydrogel, which possesses asymmetric wet adhesion, achieves interfacial adhesion by hydrogen bonds between PAA and cecum. Moreover, the smooth and antiadhesive outer layer helps prevent postoperative adhesion (Fig. 1B). The structure and physicochemical properties of Janus hydrogel was systematically characterized with SEM images, mechanical measurements, rheological property, and swelling behavior. Furthermore, the in *vitro* biocompatibility of Janus hydrogel, as well as its anti-inflammatory activities by regulating macrophage polarization and anti-fibrotic properties through modulating myofibroblast-like differentiation phenotype in PMCs, were also evaluated. Additionally, in vivo animal experiments were carried out to evaluate the anti-inflammatory effects, anti-fibrotic properties, and the inhibition capacity of collagen deposition of the Janus hydrogel in postoperative adhesion formation (Fig. 1C). Overall, the Janus hydrogel was easy to manipulate and could be applied to wet tissue surfaces without relying on other fixation materials.

2. Materials and methods

2.1. Materials

Monomers of AA, hydroxyapatite (HAP), the covalent cross-linker N, N'-methylene diacrylamide (MBAA, and Cos (molecular weight ≤2000) were purchased from Macklin (Shanghai, China). Most of Chitooligosaccharide focused molecular weight 484, containing three monosaccharide units (Fig. S1). The photoinitiator Irgacure 2959 (I2959) was purchased from Sigma. Ligu (S25473, purity ≥98 %) was purchased from Yuanye (Shanghai, China) and used as received without further purification. The primary antibodies were transforming growth factor beta 1 (TGF-β1; sc-130348, Santa Cruz, USA), Smad2/3 (AF6367, Affinity Biosciences, USA), p- Smad2/3 (AF3367, Affinity Biosciences, USA), collagen I (AF7001, Affinity Biosciences, USA), α smooth muscle actin (αSMA, bs-10196R, Bioss, China), Snail (bs-1371R, Bioss, China), E-cadherin (bs-1519R, Bioss, China), CD68 (sc-20060, Santa Cruz, USA), CD86 (FITC-65068, Proteintech, USA), CD206 (25-2061-82, Invitrogen, USA), β-actin (66009, Proteintech, USA), Diamidino-phenyl-indole (DAPI; C1002, Beyotime, China), SP Rabbit & Mouse HRP Kit (DAB; CW2069, CWBIO, China), and recombinant human TGF-β1 (ck0023, Bioss, China) were used. Second antibodies such as anti-rabbit IgG (Cy3, A0516, Beyotime, China), HRP-labeled Goat Anti-Mouse IgG (A0216, Beyotime, China) and HRP-labeled Goat Anti-Rabbit IgG (A0208, Beyotime, China) were provided. TRIzol reagent (15596018CN) was purchased from Invitrogen (CA, USA) and the qPCR kits were provided by Yeasen Co., Ltd. (Shanghai, China). Hematoxylin and eosin (H&E) staining kits and Masson's trichrome staining kits were bought from the Servicebio Co., Ltd. (Wuhan, China). The ELISA kits were purchased from Lapuda Biotech Co., Ltd. (Jiangsu, China), the live/death kit was bought from Solarbio Co., Ltd. (CA1630, Beijing, China), and the Sirius red staining kit was provided by Leagene Biotechnology Co., Ltd. (DC0041, Beijing, China).

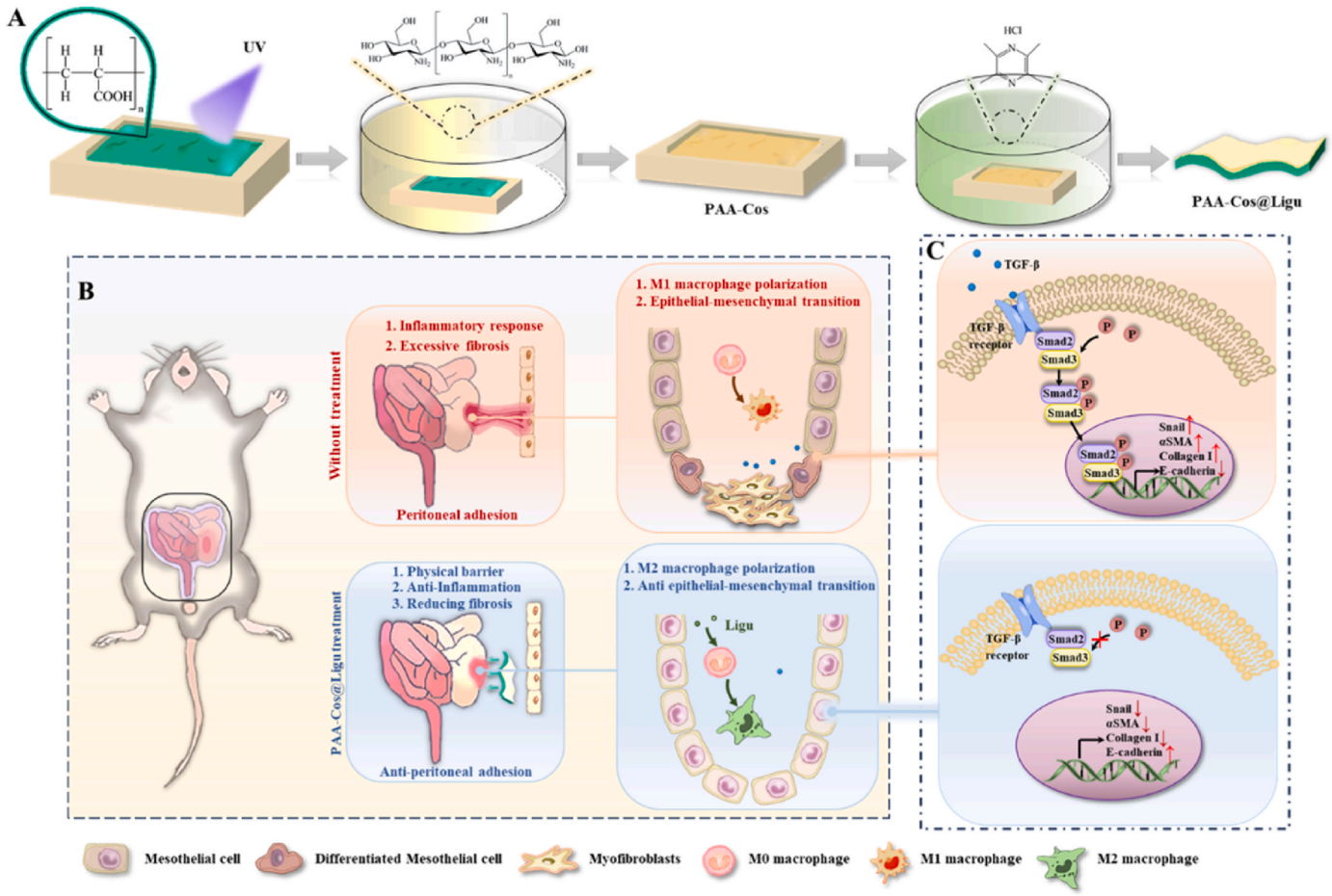

Fig. 1. A) Schematic illustration of the fabrication of the Janus hydrogel PAA-Cos@Ligu. B) The Janus bioadhesives hydrogel PAA-Cos@Ligu prevents PPA by regulating macrophage polarization and suppressing epithelial-mesenchymal transition. C) Molecular mechanism of the Janus hydrogel PAA-Cos@Ligu suppressing epithelial-mesenchymal transition through the TGF-β/Smad signaling pathway.

2.2. Synthesis of various hydrogels

The adhesive layer of PAA-Cos hydrogels (PAA hydrogel) was prepared by using a one-step method via random polymerization with AA monomers. In the procedure, the different concentrations of AA monomers were 10 %, 20 %, 30 %, and 40 % (v/v). Then, the covalent crosslinker MBAA (C_{MBAA} = 0.1 %, 0.2 %, 0.3 %, and 0.4 %; m/v), the protonating reagent HAP (0.1 %, 0.2 %, 0.3 % and 0.4 %; m/v) and photoinitiator Irgacure 2959 (1 %, 1.5 %, 2 % and 2.5 %; m/v) were added. The solution above was poured into a polytetrafluoroethylene mould and then irradiated under ultraviolet light (light intensity is 610 mW * cm^{-2}) for 5 min to light-cure the adhesive layer of hydrogels (PAA layer). The final preparation method of PAA layer was explored through single-factor and orthogonal tests.

The Janus hydrogels were obtained via a two-step method. First, to prevent two-sided PAA hydrogel from complexing with Cos solution (Mw < 2000, the concentration of Cos was 0.6 mol L^{-1}), the PAA hydrogels attached to polytetrafluoroethylene mould was immersed in Cos solution for 12 h at room temperature. Then, the above Janus hydrogels were immersed in Ligu solution to obtain PAA-Cos@Ligu hydrogels after swelling equilibrium was reached. The Cos and PAA-Cos hydrogel were analyzed by Fourier Transform Infrared Spectroscopy (FTIR) (Thermo Scientific Nicolet iN10, USA). The surface chemical compositions of the PAA-Cos hydrogel before and after soaking were analyzed by X-ray photoelectron spectroscopy (XPS) (Thermo Fisher NEXSA, USA).

2.3. Mechanical measurements

The single-factor combination of the orthogonal design method is used to conduct mechanical characterization of PAA hydrogel components and their concentrations, aiming to determine the final formulation recipe of PAA hydrogel. The orthogonal experimental design for preparing PAA hydrogel was presented in Table S1. After obtaining the PAA hydrogel, the hydrogels were immersed in deionized water; and tensile properties of PAA hydrogel were measured after swelling equilibrium was reached. The tensile properties of different PAA hydrogels were measured using a computerized tensile testing machine (TopHung TH-8203A, Suzhou) with a stretched deformation rate of 100 mm per minute.

The lap share test was performed on a computerized tensile testing machine (TopHung TH-8203A, Suzhou) to measure the adhesive strength of the Janus hydrogels in binding with wet tissue. The PAA hydrogel, PAA-Cos hydrogel, PAA-Cos@Ligu hydrogel, and intestine samples were adhered from the same end and the overlapping area was 25 mm (l) × 10 mm (w). The other two ends of the hydrogels and intestine samples were clamped, respectively, and pulled upward at a constant velocity of 50 mm per minute, and the force F was recorded. The interfacial toughness was calculated as F_{max}/area.

2.4. SEM imaging

The morphologies of PAA-Cos hydrogel were characterized by SEM (Hitachi S4800, Japan). The samples were measured in situ to observe

the real morphologies, after being immersed in deionized water. For the hydrogel samples, these were frozen at −20 °C for 4 h and freeze-dried for 24 h to remove water. Then the hydrogel samples were frozen in liquid nitrogen and then broken into pieces by hand to observe their cross-section.

2.5. Swelling ratio

To assess the swelling ratio of the various hydrogels, the different groups were lyophilized for 24 h, and then the dry weights of different groups (m_0) were weighed. After soaking each group in PBS (pH = 7.4) for 12 h, the weight (m) of the swollen hydrogels was weighed at 25 °C. The swelling ratio was confirmed by calculation based on the following equation:

$$\text{Swelling ratio } (\%) = \frac{m - m_0}{m_0} \times 100\% \quad (1)$$

2.6. Rheological properties measurements

Rheological experiments were performed on a Physica MCR-301 rheometer (ARES-G2, TA Instruments, United States) with a parallel plate (PP-10 probe, 10 mm diameter, flat). Dynamic oscillatory frequency sweep measurements were conducted at a constant strain (1 %) and frequency ranging from 100 to 1 Hz.

2.7. Cell lines and cell culture

Raw264.7 cells were bought from FuHeng Biology Co., Ltd (Shanghai, China). Human peritoneal mesothelial cells (PMCs, HMrSV5) were bought from LMAI Bio Co., Ltd. The cells were cultured with DMEM medium (Corning, USA) and RPMI 1640 medium (Corning, USA) containing 10 % fetal bovine serum (Every Green, China) and 100 U/mL penicillin/streptomycin/amphotericin in the incubator (ESCO, Singapore) under 5 % CO_2 at 37 °C, respectively.

2.8. Cell viability assay

Raw264.7 cells and PMCs were cultured in 96-well plates and allowed to attach for 12 h. The cells were cultured with a specified concentration of Ligu (25, 50, 100, 150, 200 μg/mL) for 24 h and 48 h, respectively. Subsequently, 10 μL CCK8 solution was added to each well, and the cell viability was measured under a microplate reader (Bio-Rad, USA).

2.9. Coculture assay

For co-culture analysis in a 6-well transwell chamber (8-μm pore size, Corning, Kennebunk, ME, USA), Raw264.7 and PMCs were seeded onto the lower chamber. PAA-Cos or PAA-Cos@Ligu were placed in the upper chamber. Raw264.7 and PMCs were co-cultured with PAA-Cos or PAA-Cos@Ligu for different time for the following analysis.

2.10. Cytocompatibility assay

The cytocompatibility of Raw264.7 cells co-cultured with the vehicle, PAA-Cos, or PAA-Cos@Ligu was evaluated by live/dead assay. In brief, cells were seeded at 5×10^5 cells per well in 6-well plates and co-cultured with the vehicle, PAA-Cos, or PAA-Cos@Ligu for 24 h and 72 h, respectively. After removing the old medium, the cells were washed with 1 × assay buffer and incubated with the cell viability/cytotoxicity kit away from lights for 30 min. Then the cells were visualized under a fluorescence microscope (Olympus, Japan) at random fields and representative graphs were provided.

2.11. Flow cytometry assay

To induce the polarization of macrophages, LPS (100 ng/mL, R&D Systems) + IFN-γ (20 ng/mL, Sigma) or IL-4 (20 ng/mL, R&D Systems) was used to treat Raw264.7 cells. Then, cells co-cultured with PAA-Cos or PAA-Cos@Ligu for 24 h were harvested in a dark-proof EP tube. Cells were incubated with CD86-APC (0.06 μg/10^6 cells) or CD206-PE (0.125 μg/cells) at 4 °C for 30 min and then incubated with IC fixation buffer (100 μL) at room temperature for another 30 min. Afterward, cells were washed with permeabilization buffer twice, followed by analysis using flow cytometry (Amnis, Millipore, USA).

2.12. Cytoskeletal staining

The cytoskeletal changes of Raw264.7 cells and PMCs were visualized by F-actin staining. Briefly, Raw264.7 cells co-cultured with the vehicle, PAA-Cos, or PAA-Cos@Ligu for 24 h were fixed, permeabilized, and incubated with CD206 at 4 °C overnight. Raw264.7 cells were washed with PBS containing 0.1 % Triton X-100 and then stained with Actin-Tracker Green (C2201S, Beyotime, China) the next day at room temperature for 60 min. It's said that cell membrane receptors, such as TGF-β1 could drive the transformation of PMCs into myofibroblasts. Herein, 10 ng/mL recombinant human TGF-β1 was used to stimulate PMCs for 24 h, and then PMCs were co-cultured with the vehicle, PAA-Cos, or PAA-Cos@Ligu for another 48 h, respectively. After fixation and permeabilization, PMCs were stained with Actin-Tracker Green out of light at room temperature for 60 min and then incubated with DAPI for another 5 min. Cells were blindly visualized under a fluorescence microscope (Olympus, Japan) at random fields, and representative graphs were shown.

2.13. Sirius Red staining (direct red 80)

The collagen deposition was assessed by Sirius Red staining. In brief, the PMCs were treated in different ways for 48 h as mentioned above. Then, the cells were stained with a Sirius red staining kit according to the manufacturer's instructions. For the rectum sections, the slides were incubated with 0.1 % Sirus Red solution for 1 h, and washed with 0.5 % hydrogen chloride. The collagen was stained with red, while the non-collagen was stained with orange.

2.14. Enzyme-linked immunosorbent assay (ELISA) analysis

The concentrations of IL-6 (LA128802H) and TGF-β1 (LA128806H) of cell supernatant were measured by ELISA according to the manufacturer's protocols. The optical density value was read at 450 nm wavelength. Six duplicate wells were used in each group.

2.15. Animal procedures and treatments

A total of thirty male Sprague-Dawley rats (200–220g) were provided by Dongfang Beeding Co., Ltd. (Pizhou, China). Animal experimental procedures were conducted following the institution and the Local Committee on the Care and Use of Animals of Nanjing University of Chinese Medicine (Approval No. 202208A020). Rats were randomly divided into five groups (n = 6), that is, sham, PPA, PPA-Cos, PPA-Ligu, and PPA-Cos@Ligu groups. They were acclimatized for three days in advance under standardized conditions at 20 ± 2 °C room temperature with 40 ± 5 % relative humidity and a 12 h cycle/dark cycle.

The model was prepared as our previous studies mentioned. Briefly, rats were deprived of food before the operation for about 12 h. During the operation, rats were anesthetized with 1∼1.5 % isoflurane under a supine position. After preoperative skin removal preparation, a 1.5–2 cm incision along the linea alba on the abdomen was made. The cecum was pulled out tightly and scrubbed with sterile dry gauze gently until serosal petechiae ground on the serosa layer. This grinding procedure

will last for about 5 min and about 1.0 cm × 1.0 cm wound area will be made. Then, the abraded cecum was returned to the abdomen in its natural position and the abdominal wall was sutured layer by layer. Rats in the sham group were not given abrasive surgery except for the exposure of the cecum in the air for 5 min and 200 μL saline solution was dropped onto the cecum before closing the abdominal cavity. Rats in the model group were model-prepared and the abraded cecum was dripped with 200 μL saline solution before closing the abdominal cavity. In the PAA-Cos group, the gel without Ligu was stuck on the abraded cecum of rats before closing the abdominal cavity. In the PPA-Ligu group, Ligu solution (2 mg/kg) was dropped onto the injured cecum before closing the abdominal cavity. In the PAA-Cos@Ligu group, the gel with Ligu (6 mg/kg) was stuck on the abraded cecum of rats before closing the abdominal cavity. Rats were anesthetized with 1∼1.5 % isoflurane and cervical dislocation on day 7 post-surgery. After supine position fixation, rats underwent an inverted U-shaped incision on the abdomen. The injured cecum surrounding adhesive sites were harvested for the following studies.

2.16. Gross observation and adhesion scoring

The peritoneal adhesions were observed and photographed by a bystander who was blind to the study design. The adhesion was scored in a double-blind scoring way according to previous studies. Score 0, no adhesion; score 1, 0–25 % thin, avascular, and transparent adhesion area; score 2, 25–50 % thin, avascular, and transparent adhesion area; score 3, 50–75 % thick and opaque adhesion area with capillaries which required sharp dissection; score 4, 75–100 % thick and opaque adhesion area with large vessels which required sharp dissection.

2.17. Histopathological staining

A portion of the cecum tissue was fixed with 4 % paraformaldehyde for 24 h, embedded into the paraffin, and sectioned into 4 μm-thick sections. Then, the sections were stained with Hematoxylin & eosin (HE) and Masson's trichrome Staining, respectively. The images were blindly examined at random fields under a microscope (Olympus, Japan).

2.18. Immunofluorescent staining

After the cecum slides were dewaxed and dehydrated step by step, the specimens were blocked with QuickBlock™ blocking buffer (P0260, Beyotime, China), followed by incubation with the primary antibodies against αSMA (1:200), and CD68 (1:200) overnight at 4 °C. Then, the sections were washed with PBS twice in 5 min and incubated with the secondary antibodies in the dark for 1 h. The nuclei of cells were stained by DAPI for 5 min at room temperature.

For staining with cells, LPS + IFN-γ or IL-4 was used to induce the polarization of macrophages. Raw264.7 cells co-cultured with PAA-Cos, or PAA-Cos@Ligu for 24 h were fixed with pre-cooled 4 % paraformaldehyde for 15 min and then stained with the primary antibodies CD86 (100 μL/10^6 cell) or CD206 (1:200) for 2 h at room temperature. Afterward, cells were incubated with secondary antibodies for 1 h and stained with DAPI for another 5 min in the dark. Regarding the PMCs, PMCs were seeded in 24-well plates and treated differently as above for 48 h. Cells were incubated with αSMA (1:200) and secondary antibodies as the above protocol. After the nuclei of cells were stained, the stained images were blindly imaged at random fields under a fluorescence microscope (Olympus, Japan). The expression of αSMA and CD68 were semiquantitatively measured by ImageJ software.

2.19. Histological immunohistochemistry staining

After the cecum tissues were deparaffinized and rehydrated with grades of ethanol, the slides were stained followed by DAB's instructions. In brief, the sections were immunostained with primary antibodies, i.e. rabbit anti-αSMA (1:200), and mouse anti-CD68 (1:200) overnight at 4 °C, followed with the secondary antibodies for 10 min at room temperature. The colors were viewed by DAB and then the slides were counterstained with hematoxylin. Following dehydration by ethanol and xylene step by step, the images were blindly observed at random fields under a microscope (Olympus, Japan). The expression of CD68 and αSMA were quantified by ImageJ software.

2.20. Western blotting analysis

Protein was extracted by using RIPA Lysis Buffer (P0013B, Beyotime, China), quantified, and boiled in the water bath at 100 °C for 10 min with 1 × SDS-PAGE sample loading buffer. Equivalent samples were subjected to 10 % precast protein plus gel (Yeasen, China) and transferred to polyvinylidene fluoride (PVDF) membranes. The membranes were blocked in 5 % silk milk for 80 min and incubated with primary antibodies against Smad2/3 (1:1000), p-Smad2/3 (1:1000), TGF-β1 (1:500), collagen I (1:500), Snail (1:1000), E-cadherin (1:1000) and αSMA (1:1000). And actin (1:10000) was selected as internal controls. The secondary antibodies including HRP-labeled Goat Anti-Mouse IgG (1:1000) and HRP-labeled Goat Anti-Rabbit IgG (1:1000) were used. The bands were visualized by the Chemiluminescence Imaging System (Bio-Rad, USA), and the gray value was analyzed by ImageJ software.

2.21. qRT-PCR analysis

The Smad2, Smad3, TGF-β1, IL-1β, IL-6, TNF-α, collagen I, Snail, E-cadherin, and αSMA mRNA levels were measured by qRT-PCR. GAPDH was selected as an internal control. The total RNA of the cecum tissue and cell sample was extracted, synthesized, quantified, and amplified according to the instructions. The primers were designed in Tsingke Co., Ltd. (Beijing China). The sequences of primer pairs were listed as follows (Table S2). The relative transcription levels of target genes were measured by using the comparative Ct ($2^{-\Delta\Delta Ct}$) method.

2.22. Statistical analysis

Data were analyzed by SPSS 25.0 software (Chicago, USA) and were shown as mean ± standard deviation (SD). A One-way ANOVA test with an LSD test was used for normally distributed continuous data and the Kruskal-Wallis test was applied for the abnormally distributed data. $P < 0.05$ was considered significant.

3. Results and discussion

3.1. Preparation and characterization of PAA-Cos and PAA-Cos@Ligu

In this study, the Janus hydrogel was obtained via a two-step method. After comparing the tensile strength of different PAA hydrogel, the concentrations of AA monomers were 40 % (v/v) with the covalent cross-linker MBAA (C_{MBAA} = 0.1 %; m/v), the protonating reagent HAP (0.1 %; m/v) and photoinitiator Irgacure 2959 (1.5 %; m/v) to prepare the adhesive layer of Janus hydrogels. First, the adhesive layer of Janus hydrogels (PAA hydrogel) was prepared by the one-pot polymerization of AA in the polytetrafluoroethylene mould. After attached tightly to polytetrafluoroethylene mould, PAA hydrogel was immersed in Cos solution for 12 h at room temperature. This method would allow Cos to diffuse into the top surface of PAA hydrogel and complex together via the electrostatic interaction, while preventing Cos contact to the bottom surface of PAA hydrogel, finally obtaining the Janus hydrogel of PAA-Cos. To prepare PAA-Cos@Ligu, PAA-Cos was further immersed in ligustrazine hydrochloride solution, which allowed Ligu to diffuse into the PAA-Cos until the swelling equilibrium was reached. It could be found that PAA-Cos showed a distinct diffusion layer of Cos in PAA hydrogel with color gradients from deep (top surface) to shallow (bottom surface) (Fig. 2A). Meanwhile, the SEM images

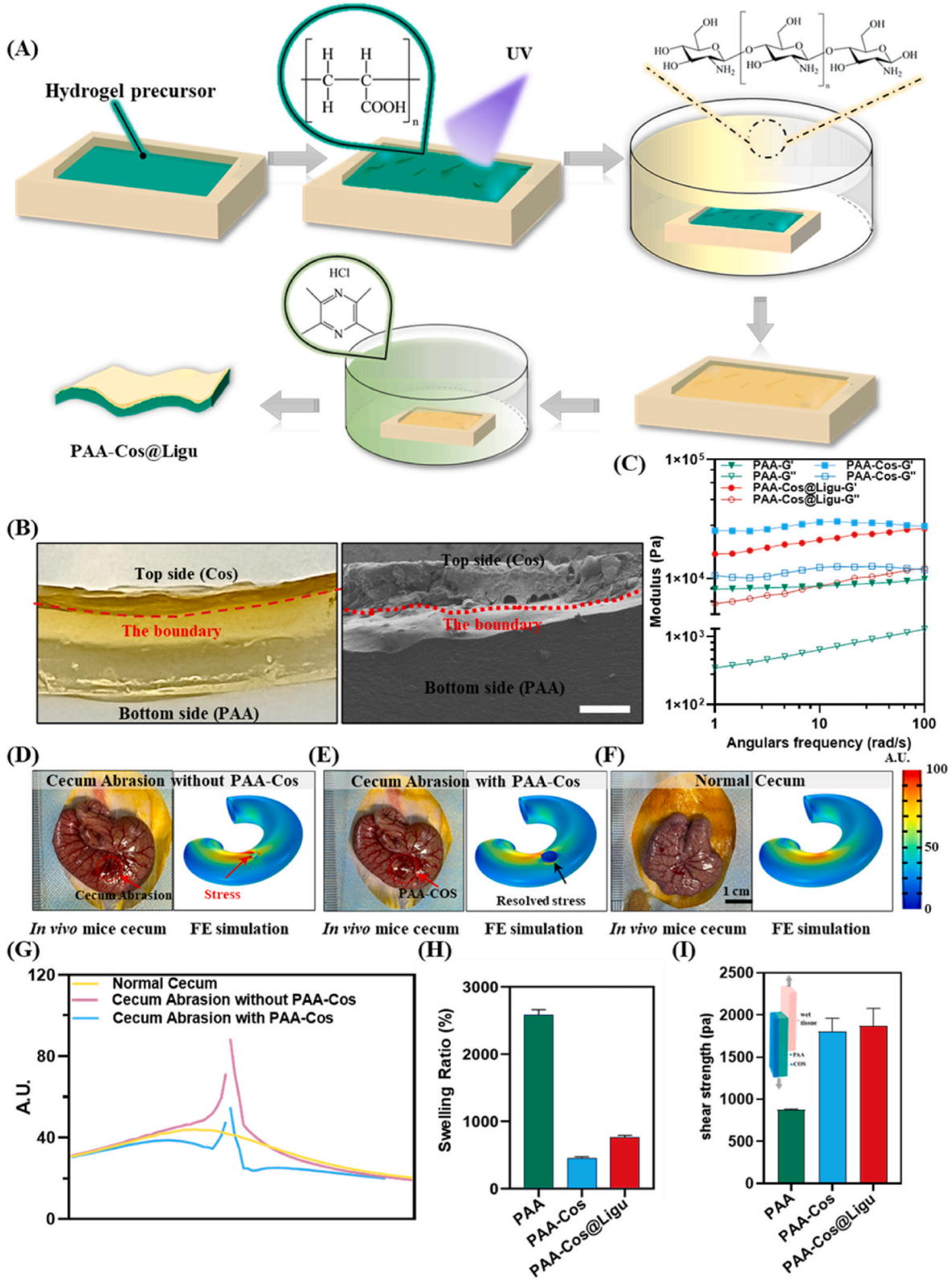

Fig. 2. Preparation and characterization of PAA-Cos and PAA-Cos@Ligu. A) Schematic illustration of the preparation of the Janus hydrogel PAA-Cos@Ligu. B) Image and SEM images of the cross-section of the Janus hydrogel PAA-Cos. Scale bar: 50 μm. C) The storage moduli (G′) and loss moduli (G″) of PAA, PAA-Cos and PAA-Cos@Ligu. D) In *vivo* cecum abrasion and finite-element results of mechanical stress on the rat. E) In *vivo* cecum abrasion and mechanical modulation of the corresponding finite-element results by PAA-Cos. F) In *vivo* normal cecum and mechanical modulation of the corresponding finite-element results. Contraction of wound and wound-edge stress concentration are exhibited in the experimental photo and finite-element results. G) Statistics of wound-edge stress or normal cecum stress in different groups. H) Swelling ratio (%) of the PAA, PAA-Cos, and PAA-Cos@Ligu. I) Shear strength of the PAA, PAA-Cos, and PAA-Cos@Ligu on wet rat skin.

also revealed that PAA-Cos possessed a structure containing irregular holes distributed in the top side, but compact structure in the bottom side (Fig. 2B), suggesting that the PAA cross-linked by MBAA would enhance the hydrogel network. For PAA-Cos@Ligu, Ligu would crystallize from the PAA-Cos@Ligu during lyophilization, thus the crystal of Ligu could be found from SEM images **(**Fig. S2**)**.

Next, the rheological property of different hydrogels was also evaluated. The results showed that all the hydrogels including PAA, PAA-Cos, and PAA-Cos@Ligu exhibited stable hydrogel characteristics with the storage modulus (G′) higher than the loss modulus (G″) (Fig. 2C). Additional crosslinking points of electrostatic interaction may form at the interface between PAA and Cos, further enhancing the gel strength of the PAA-Cos hydrogel. The gel strength of PAA-Cos and PAA-Cos@Ligu significantly enhanced when compared to that of PAA (Fig. 2C). To prepare PAA-Cos@Ligu, the PAA-Cos was hydrogel soaked in Ligu solution, which leading to the strength of PAA-Cos@Ligu lower than that of PAA-Cos. Finite-element analyses (FEA) was used to further explore the suitability of PAA-Cos for PPA. Photographic evidence revealed that PAA-Cos could adhere to the damaged cecum of rats well (Fig. 2D–F). FEA also demonstrated that the adhibition of PAA-Cos could reduce stresses concentrated around the wound edge, thus promoting wound healing (Fig. 2D–F). The statistical strength theory around the cecum wound edge in the PAA-Cos group was consistent with normal cecum tissue (Fig. 2G). In addition, it could be found that the swelling ratio of PAA hydrogel was remarkably higher than that of PAA-Cos and PAA-Cos@Ligu. The reason would be due to the polyelectrolyte complexation between polyanionic PAA and polycationic Cos, which increased the crosslink density of the network and contributed to stabilizing the hydrogel (Fig. 2H). Meanwhile, PAA-Cos loaded with Ligu would lead to a decrease in gel strength, but an increase in swelling ratio, which might be due to the part replacement of Cos by positive Ligu in the PAA-Cos. Besides, the adhesion property of the bottom surface to wet tissue was also investigated by detecting the shear strength. As shown in Fig. 2I, the shear strength of PAA-Cos and PAA-Cos@Ligu was significantly higher than that of PAA, indicating that the Janus hydrogel of PAA-Cos and PAA-Cos@Ligu could tightly adhere to the wet tissue. It had been reported that the polyelectrolyte complexes formed inside of PAA-Cos and PAA-Cos@Ligu would promote the phase separation, which could reduce the interface energy and increase the hydrophobicity of the layer approaching the bottom surface, finally expelling water between the bottom surface and wet tissue and triggering the adhesion of the remaining carboxyl groups to the wet tissue. Thus, the above results indicated that both PAA-Cos and PAA-Cos@Ligu possessed the characteristic of Janus hydrogel with asymmetric adhesion on the two faces.

3.2. *In vitro biocompatibility, polarization of macrophages and anti-inflammatory activities by PAA-Cos@Ligu*

The live/death assay was used to evaluate the cytocompatibility of the above hydrogels during the co-culture period. As shown in Fig. 3A, compared to vehicles, no significant difference was found in Raw264.7 cells after co-cultured with PAA-Cos or PAA-Cos@Ligu for 24 and 72 h, indicating that the composed of PAA-Cos or PAA-Cos@Ligu had good biocompatibility. It's well known that macrophages play pivotal roles in the occurrence and progression of inflammation. A previous study found that polarization of macrophages was linked to adhesion formation [32]. Thus, the polarization of macrophage as well as the anti-inflammatory effect of PAA-Cos@Ligu on Raw264.7 cells was investigated. CD86 and CD206 are typical markers of M1 and M2 macrophage phenotypes. As presented in Fig. 3B–D, the immunofluorescence images indicated that Raw264.7 cells obviously trended to express CD206 rather than CD86 when treated by PAA-Cos@Ligu, as a significant difference was found in CD86 expression between LPS + IFN-γ and PAA-Cos@Ligu group ($p < 0.01$), and the immunofluorescence intensity of CD206 in the PAA-Cos@Ligu group was similar to that in the IL-4 group ($p > 0.05$). In addition, the results of flow cytometry were consistent with the immunofluorescent staining (Fig. 3E). The proportion of M2 macrophages reached 96.2 ± 1.9 % when treated by PAA-Cos@Ligu and was similar to that in the IL-4 group, while the proportion of M1 macrophages only accounted for about 24.8 ± 13.0 % in PAA-Cos@Ligu, which was significantly lower than LPS + IFN-γ group ($p < 0.01$). Furthermore, the cytoskeleton of Raw264.7 cells stained with F-actin indicated the morphologic change of Raw264.7 cells treated by PAA-Cos@Ligu was similar to the IL-4 group (Fig. 3F), suggesting that more macrophages were polarized into M2 macrophage phenotype. Meanwhile, there was no significant difference in the supernatant level of M2-associated anti-inflammatory cytokines (TGF-β1) in the PAA-Cos@Ligu group when compared with the IL-4 group ($p > 0.05$) (Fig. 2G). Altogether, the above results exhibited that PAA-Cos@Ligu could induce macrophage polarization toward the M2 phenotype and exert anti-inflammatory functions.

3.3. *In vitro decrease of myofibroblast-like differentiation and collagen deposition in peritoneal mesothelial cells by PAA-Cos@Ligu*

PMCs are the primary barrier of the abdominal cavity, which exert unique roles in the occurrence and development of peritoneal adhesion. Previous reports found that PMCs participated in the activation of myofibroblast with phenotypic change and altered αSMA and collagen deposition [17]. Thus, the phenotypic responses and collagen deposition of PMCs co-cultured with PAA-Cos@Ligu were performed. Represented morphology images of PMCs showed that PMCs possessed round shapes with small diameters, while cells with more elongated or spindle morphology, as well as longer diameters (70.1 ± 17.6 μm) were observed when stimulated with TGF-β1. However, compared with the TGF-β1 group, cells co-cultured with PAA-Cos or PAA-Cos@Ligu showed fewer morphologic changes with smaller diameters about 43.5 ± 20.1 μm and 42.1 ± 18.7 μm, respectively (Fig. 4A and B). The results indicated the possibility of a transition process from mesothelial cells toward myofibroblast-like phenotypic changes during peritoneal adhesion [33] which could be inhibited after the application of PAA-Cos or PAA-Cos@Ligu. αSMA is a typical marker of myofibroblasts. As presented in Fig. 4C, the expression of αSMA was dramatically increased in the TGF-β1 group in comparison with the control group. After co-culturing with the bioadhesives, especially with PAA-Cos@Ligu, the expression of αSMA was remarkably decreased. Similar results were also found in the immunofluorescence intensity analysis (Fig. 4D). In addition, significantly positive staining of direct Red 80 was observed in PMCs after pre-treated with TGF-β1, while the staining of direct Red 80 was weakened when co-cultured with bioadhesives (Fig. 4E). As displayed in Fig. 4F, the semi-quantitative results of direct Red 80 staining also indicated that the expression of collagen deposition was notably elevated in the TGF-β1 group (0.9 ± 0.1) when compared with the vehicle group (0.1 ± 0.0). After treating with bioadhesives, especially with PAA-Cos@Ligu, the levels of collagen deposition were remarkably reduced (0.5 ± 0.1, $p < 0.01$). Based on the above evidence, we further inferred the potential effects of PAA-Cos@Ligu on the myofibroblast-like differentiation of PMCs, the protein levels, and mRNA expressions of mesenchymal-related phenotypic markers (Snail, αSMA, and collagen I), and mesothelial-associated phenotypic markers (E-cadherin) were determined. As shown in Fig. 4G and H, the protein expressions of Snail, αSMA, and collagen I were notably increased, and the protein level of E-cadherin was significantly decreased compared to the vehicle group, indicating a myofibroblast-like differentiation when stimulated with TGF-β1. After being treated with the bioadhesives, the expressions of the above indicators were notably reversed with a decrease of Snail, αSMA, and collagen I, while increase of E-cadherin when compared with the TGF-β1 group. A similarly reversed trend was also observed in the mRNA expressions of Snail, αSMA, collagen I, and E-cadherin when co-cultured by PAA-Cos and PAA-Cos@Ligu (Fig. 4I). Collectively, the above findings suggested that PAA-Cos@Ligu might inhibit the myofibroblast-like phenotypic changes and collagen deposition of PMCs when induced with

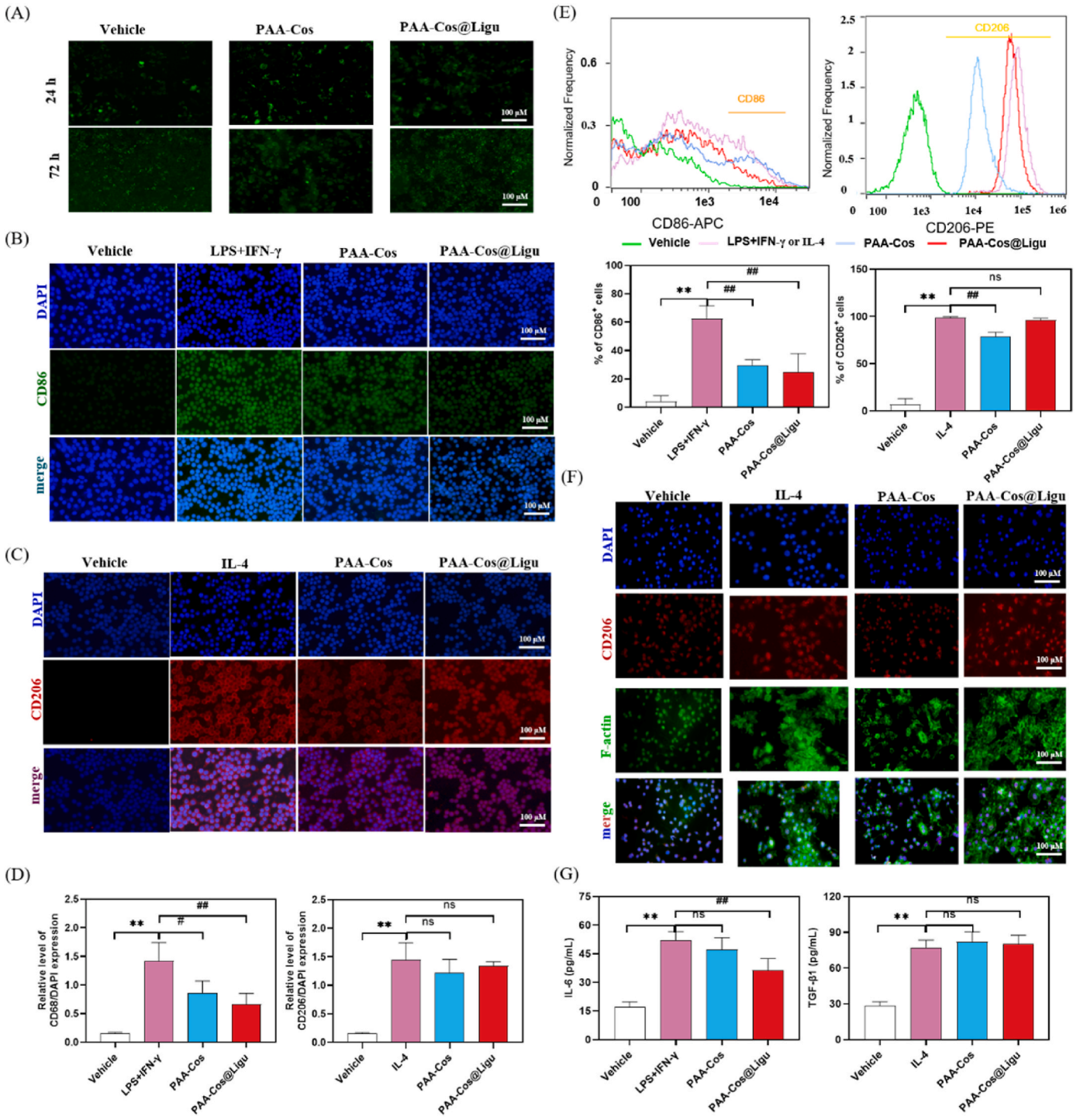

Fig. 3. In *vitro* biocompatibility, polarization of macrophages, and anti-inflammatory activities by PAA-Cos@Ligu. A) Representative images of Raw264.7 cells with live/death assay after incubation with Cos-Ligu or PAA-Cos@Ligu for 24 h or 72 h. Scale bar = 100 μm. B and C) Immunofluorescence images of M1/M2 marker (CD86/CD206) expression in Raw264.7 cells pre-treated with LPS + IFN-γ or IL-4 for 24 h and then incubated with Cos-Ligu or PAA-Cos@Ligu for another 24 h. Scale bar = 100 μm. D) Immunofluorescence intensity of M1/M2 marker (CD86/CD206) expression in Raw264.7 cells pre-treated with LPS + IFN-γ or IL-4 for 24 h and then incubated with Cos-Ligu or PAA-Cos@Ligu for another 24 h, n = 3 per group. E) Flow cytometry analysis of M1/M2 marker (CD86/CD206) expression in Raw264.7 cells pre-treated with LPS + IFN-γ or IL-4 for 24 h and then incubated with Cos-Ligu or PAA-Cos@Ligu for another 24 h, n = 3 per group. F) Fluorescence images of CD206 and F-actin in Raw264.7 cells pre-treated with IL-4 for 24 h and then incubated with Cos-Ligu or PAA-Cos@Ligu for another 24 h. Scale bar = 100 μm. G) ELISA assay of M1-associated pro-inflammatory cytokines (IL-6) and M2-associated anti-inflammatory cytokines (TGF-β1) in the supernatant of Raw264.7 cells pre-treated with LPS + IFN-γ and IL-4 for 24 h, respectively, and then incubated with Cos-Ligu or PAA-Cos@Ligu for another 24 h, n = 6 per group. Compared with the vehicle group, $^{*}P < 0.05$, $^{**}P < 0.01$. Compared with the LPS + IFN-γ or IL-4 group, $^{\#}P < 0.05$, $^{\#\#}P < 0.01$.

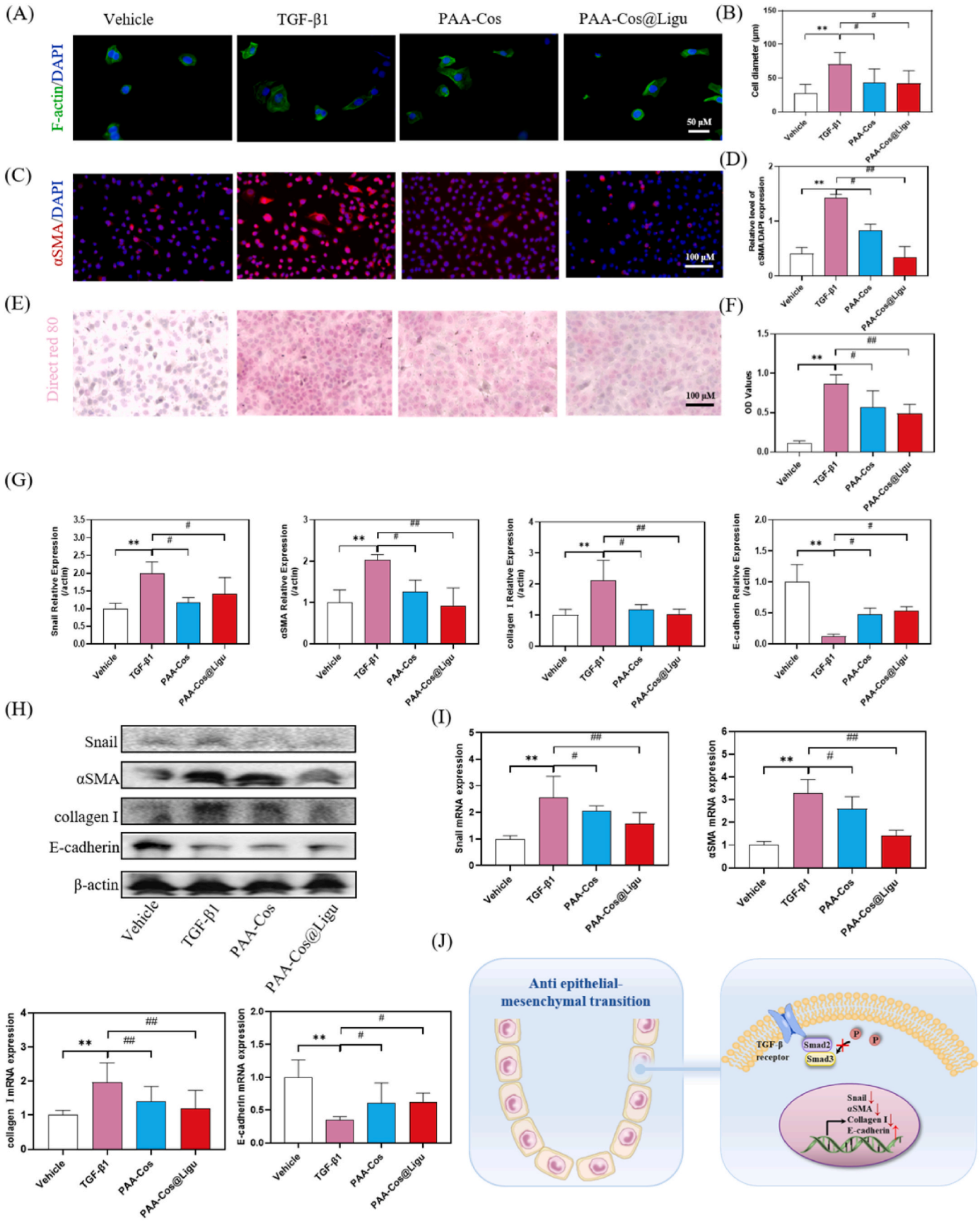

(caption on next page)

Fig. 4. In *vitro* decrease of myofibroblast-like differentiation and collagen deposition in peritoneal mesothelial cells by PAA-Cos@Ligu. A) F-actin staining assay of the cytoskeletal phenotype of PMCs after treated with different groups. Scale bar = 50 μm. B) The cellular diameter of the cytoskeletal phenotype of PMCs after treated with different groups. n = 6 per group. C) Immunofluorescence assay of αSMA in PMCs after treated with different groups. Scale bar = 100 μm. D) The fluorescence intensity assay of αSMA in PMCs after treated with different groups. n = 3 per group. E) Direct red 80 staining in PMCs after treated with different groups. Scale bar = 100 μm. F) The semi-quantitative assay of Direct red 80 staining in PMCs after treated with different groups. n = 3 per group. G and H) Western blot of mesenchymal-related phenotypic markers (Snail, αSMA, and collagen I) and mesothelial-associated phenotypic markers (E-cadherin). n = 3 per group. I) qRT-PCR analysis of mesenchymal-related phenotypic markers (Snail, αSMA, and collagen I) and mesothelial-associated phenotypic markers (E-cadherin). n = 6 per group. J) Schematic diagram illustrating the effect of PAA-Cos@Ligu on myofibroblast-like differentiation and collagen deposition. Compared with the vehicle group, $^{*}P < 0.05$, $^{**}P < 0.01$. Compared with the TGF-β1 group, $^{\#}P < 0.05$, $^{\#\#}P < 0.01$. (For interpretation of the references to color in this figure legend, the reader is referred to the Web version of this article.)

TGF-β1 (Fig. 4J).

3.4. In vivo anti-peritoneal adhesive effects by PAA-Cos@Ligu

To determine the anti-peritoneal adhesive effects of PAA-Cos@Ligu in *vivo*, an established rodent model of peritoneal adhesion in SD rats was used [18,32] and a simple diagram was shown in Fig. 5A. The incisions of all rats were healed without infection or complication during the model preparation. There was no significant difference on day 1, day 4, and day 7 in the body weight of all five groups (Fig. S9). All rats were sacrificed on the 7th day after model preparation. The frequency of different grades among groups and adhesion scores were presented in Fig. 5B–C. There was a significant increase in the adhesion score for PPA-Cos with severe adhesive area when compared with the sham group, but a significant decrease when compared with the model group. Similar results were also found when treated with free Ligu. The abraded cecum treated with the PAA-Cos@Ligu had a prominently lower adhesion score when compared with the PPA-Cos and free Ligu. The adhesion scores were listed as follows: Model > Ligu > PPA-Cos > PPA-Cos@Ligu > Sham. Meanwhile, the represented views of peritoneal adhesion and HE staining showed that only slight peritoneal adhesive could be found when treated by PPA-Cos@Ligu (Fig. 5D–E), indicating that PPA-Cos@Ligu possessed the capacity of anti-peritoneal adhesive.

To evaluate the collagen deposition in the abraded cecum, both Masson staining and Sirus red staining were conducted on the tissue sections. As shown in Fig. 5F and G, Masson staining and Sirus red staining exhibited that massive collagens were deposited in the model group when compared with the sham group, while there was a dramatically decreased collagens deposition when treated with the bioadhesives when compared to the model group. Notably, the PAA-Cos@Ligu group showed less collagen fiber deposition in comparison with PAA-Cos or free Ligu. Similar results could be found in the semi-quantitative assay of Masson staining and Sirus red staining (Fig. 5H and I). Besides, the mRNA expressions of TGF-β1 also showed that the model group could significantly upregulate the level of TGF-β1, while treatment with PAA-Cos@Ligu could significantly downregulate the level of TGF-β1 (Fig. 5J). All the above results revealed that PAA-Cos@Ligu could reduce collagen deposition in the abraded cecum.

To further investigate whether PAA-Cos@Ligu could exhibit anti-inflammatory action, the level of inflammation-associated cytokines was detected by qRT-PCR. Compared with the sham group, the mRNA expressions of IL-1β, IL-6, and TNF-α in the model group significantly increased. After treatment with PAA-Cos@Ligu, the mRNA levels of IL-1β, IL-6, and TNF-α markedly decreased in comparison with the model group (Fig. 5K). Together, these findings reflected that PAA-Cos@Ligu could remarkedly attenuate peritoneal adhesion by suppressing collagen deposition and inflammatory action.

3.5. In vivo decrease of myofibroblast-like changes and inhibition of TGF-β/Smad2/3 signaling by PAA-Cos@Ligu

Previous studies have shown that myofibroblasts, which secret adhesion collagen, are driven from mesothelial cells [14]. While αSMA-positive myofibroblast, persistently secreting collagen, is referred to as one of the biomarkers in various fibrotic disorders [34]. $CD68^{+}$ macrophages can undergo myofibroblast-like changes with collagen generation and contribute to myofibroblast formation in fibrosis [33]. Herein, we probed the co-expression of macrophages and myofibroblast markers by identifying double-labeling CD68 and αSMA in adhesive tissues. As presented in Fig. 6A, the double immunofluorescent analysis demonstrated that the fluorescence intensity of $CD68^{+}$ and αSMA^{+} in the model group were higher than those in the sham group. After treatment with bioadhesives, especially for PAA-Cos@Ligu, the fluorescence intensity of $CD68^{+}$ and αSMA^{+} significantly declined. While no obvious effect on the decrease of the fluorescence intensity was found when treated with free Ligu (Fig. 6B–C). The immunohistochemical analysis further verified the findings above. As shown in Fig. 6D–F, the $CD86^{+}$ staining area, accounting for approximately 11.2 ± 1.8 % of the model group, was higher than that in the sham group with a proportion of 2.4 ± 0.8 %. This ratio was markedly reduced to 2.4 ± 1.9 % in the PAA-Cos@Ligu group. Similarly, the αSMA positive staining area with a proportion of 27.0 ± 1.4 % in the model group was notably higher than that in the sham group with a proportion of 10.4 ± 0.3 %. After treatment with PAA-Cos@Ligu, the percentage of the positive staining area declined to 8.2 ± 2.8 %. All the above results demonstrated that PAA-Cos@Ligu could decrease myofibroblast-like changes, thereby decreasing the production of fibrotic collagen and suppressing adhesion formation.

TGF-β/Smad signaling is regarded as the major regulatory factor in tissue fibrosis [35]. Overexpressed levels of TGF-β1 in the peritoneum showed a positive correlation with the increased incidence of adhesion [36]. The downstream of Smad, is a group of intracellular proteins, that serve as the critical mediators of TGF-β1 signaling, facilitating the transmission of signals from the cell surface to the nucleus, thereby promoting the transcription of target genes [37]. To explore the critical effect of PAA-Cos@Ligu on the downstream of TGF-β1 and Smad2/3, the western blot and qRT-PCR experiment were performed. As shown in Fig. 6G–H, there was no statistical difference in the expression of Smad2/3 protein among different treated groups ($p > 0.01$). In comparison with the sham group, the protein levels of p-Smad2/3, TGF-β1, collagen I, and αSMA were significantly upregulated in the model group (all $p < 0.01$). After treatment with PAA-Cos@Ligu, p-Smad2/3, TGF-β1, collagen I and αSMA levels were markedly downregulated when compared with the model group (all $p < 0.01$). The results were in line with those of qRT-PCR (Fig. 6I). Compared with the sham group, the mRNA expressions of Smad2, Smad3, TGF-β1, collagen I, and αSMA in the model group significantly increased. After treatment with PAA-Cos@Ligu, the mRNA levels of Smad2, Smad3, TGF-β1, collagen I, and αSMA decreased markedly (all $p < 0.01$) in comparison with the model group. Taken together, these discoveries indicated that PAA-Cos@Ligu could lessen adhesion formation by inhibiting TGF-β/Smad2/3 signaling to decrease the production of fibrotic collagen.

4. Conclusion

In this study, we first developed a Janus hydrogel (PAA-Cos@Ligu) that possesses the capability to adhere to wet tissues robustly and prevent PPA simultaneously. Compared to conductive hydrogels [38] and electrospun fibers [39], the unique dual-sided properties of Janus

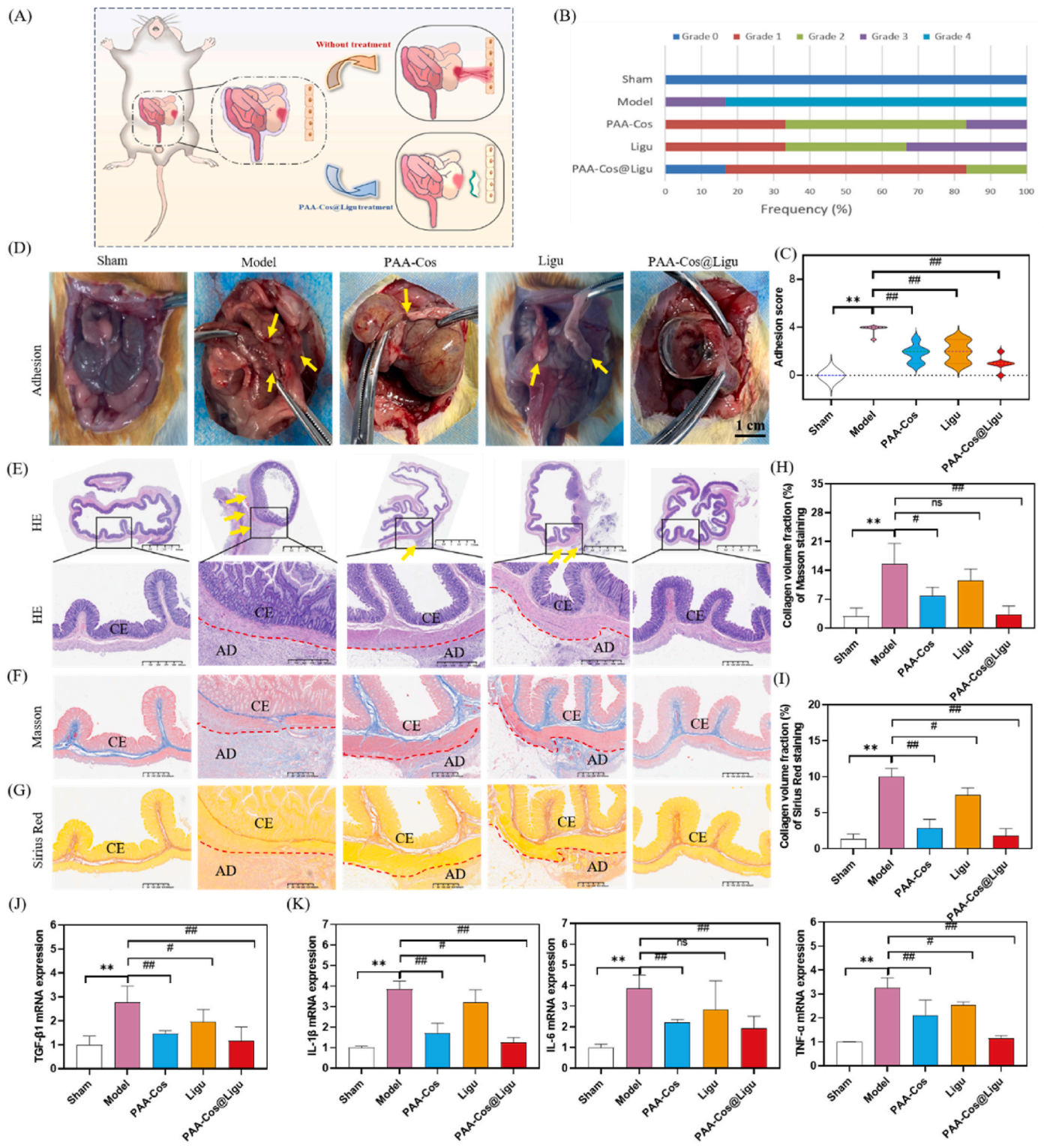

Fig. 5. In *vivo* anti-peritoneal adhesive effects by PAA-Cos@Ligu. A) Schematic illustrations of the application of PAA-Cos@Ligu on a rat cecum-abdominal wall adhesion model. B) Adhesion frequency of different treated groups. n = 6 per group. C) Adhesion scores of different treated groups. n = 6 per group. D and E) Representative images of adhesion formation and HE staining of cecum sections in different treated groups. Yellow arrows show the adhesion between abdominal wall and cecum in gross observation. CE: cecum, AD: adhesion. Scale bar = 400 μm. F) Masson staining of cecum sections in different treated groups. CE: cecum, AD: adhesion. Scale bar = 400 μm. G) Sirius Red staining of cecum sections in different treated groups. CE: cecum, AD: adhesion. Scale bar = 400 μm. H) Collagen volume fraction of Masson staining of cecum sections in different treated groups. n = 3 per group. I) Collagen volume fraction of Sirius Red staining of cecum sections in different treated groups. n = 3 per group. J) qRT-PCR analysis of TGF-β1 of cecum sections in different treated groups. n = 4 per group. K) qRT-PCR analysis of IL-1β, IL-6, and TNF-α of cecum sections in different treated groups. n = 4 per group. Compared with the sham group, $^{*}P < 0.05$, $^{**}P < 0.01$. and Compared with the model group, $^{\#}P < 0.05$, $^{\#\#}P < 0.01$. (For interpretation of the references to color in this figure legend, the reader is referred to the Web version of this article.)

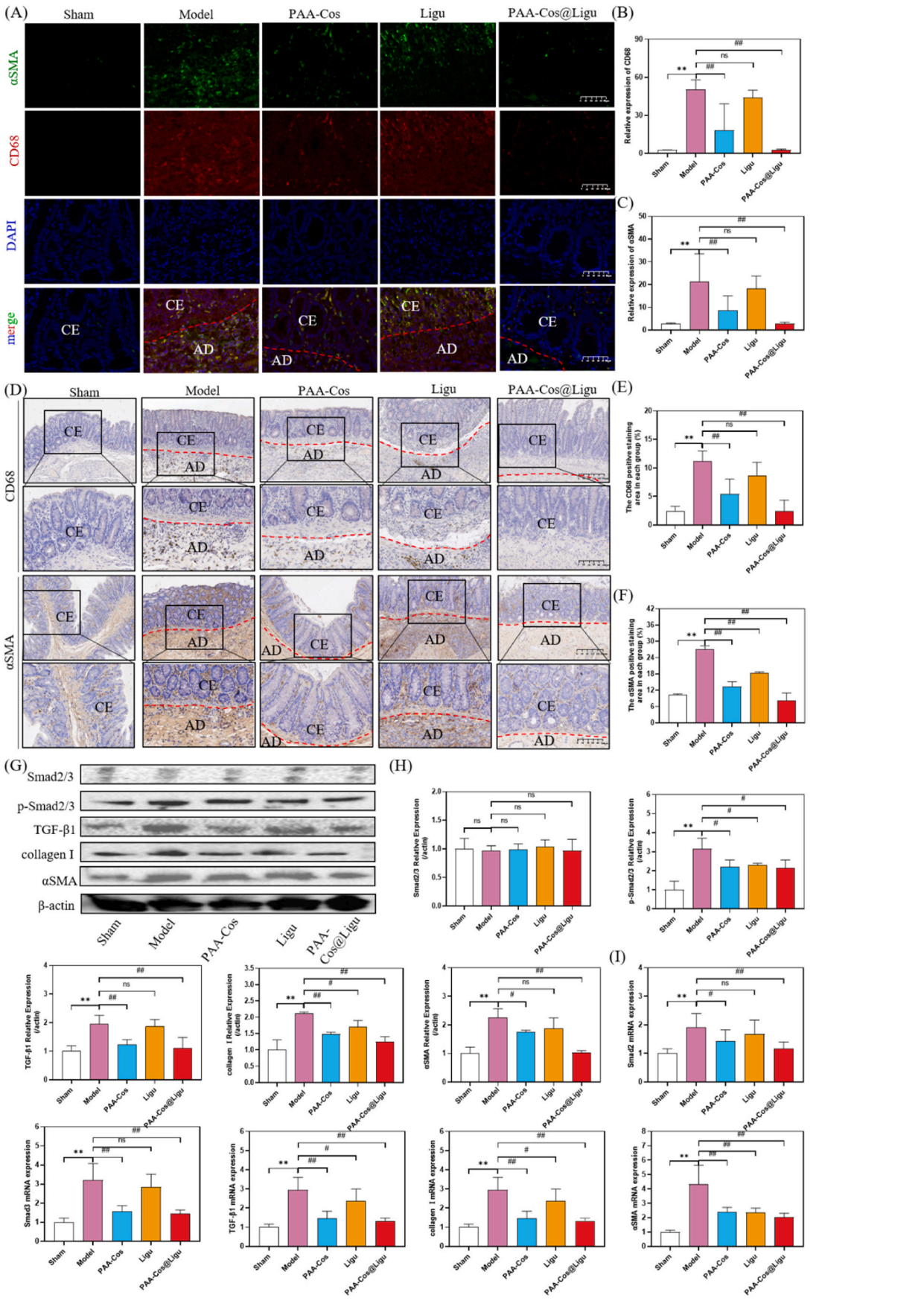

(caption on next page)

Fig. 6. In *vivo* decrease of myofibroblast-like changes and inhibition of TGF-β/Smad2/3 signaling by PAA-Cos@Ligu. A) Immunofluorescence images of CD68 (green) and αSMA (red) of cecum sections in different treated groups. CE: cecum, AD: adhesion. Scale bar = 50 μm. B) The fluorescence intensity assay of CD68 in different treated groups. n = 3 per group. C) The fluorescence intensity assay of αSMA in different treated groups. n = 3 per group. D) immunohistochemical images of CD68 and αSMA of cecum sections in different treated groups. CE: cecum, AD: adhesion. Scale bar = 200 μm and Scale bar = 100 μm. E) The positive staining area assay of CD68 in different treated groups. n = 3 per group. F) The positive staining area assay of αSMA in different treated groups. n = 3 per group. G-H) Western blot of Smad2/3, p-Smad2/3, TGF-β1, collagen I, and αSMA of cecum sections in different treated groups. n = 3 per group. I) qRT-PCR analysis of p-Smad2/3, TGF-β1, collagen I, and αSMA of cecum sections in different treated groups. n = 3 per group. Compared with the sham group, $^{*}P < 0.05$, $^{**}P < 0.01$. Compared with the model group, $^{\#}P < 0.05$, $^{\#\#}P < 0.01$. (For interpretation of the references to color in this figure legend, the reader is referred to the Web version of this article.)

hydrogels — where the adhesive layer tightly adheres to wet tissue, and the anti-adhesive layer serves as a physical barrier — endow them with potential applications in tissue repair, particularly in the field of post-operative adhesion prevention. This PAA-Cos@Ligu exhibits excellent cytocompatibility, anti-inflammatory effects by modulating macrophage polarization, and anti-fibrosis by inhibiting myofibroblast-like phenotype and collagen deposition, finally resulting in effectively preventing PPA in *vivo*. Furthermore, the mechanism of PAA-Cos@Ligu to reduce adhesion formation would be due to the suppression of the TGF-β/Smad2/3 signaling pathway. Thus, we conclude that PAA-Cos@Ligu possesses considerable promise as a premier barrier material for preventing postoperative adhesions with good biocompatibility. However, this study had certain limitations. Firstly, we were unable to conclusively determine whether decreasing the production of TGF-β or inhibiting the downstream effects of TGF-β is the primary mechanism for preventing peritoneal adhesions. Additionally, PAA-Cos@Ligu has shown the capability to reduce PPA by inhibiting the TGF-β/Smad2/3 signaling pathway. However, other potential pathways involved in PPA formation were not investigated in this study. Lastly, although PAA-Cos@Ligu has demonstrated effectiveness in preventing peritoneal adhesions both in *vivo* and in *vitro*, further clinical trials are necessary to confirm its efficacy in preventing PPA in humans.

CRediT authorship contribution statement

Zhengjun Li: Writing – original draft, Validation, Methodology, Funding acquisition, Conceptualization. **Lili Yang:** Writing – original draft, Methodology, Investigation, Funding acquisition, Formal analysis, Data curation, Conceptualization. **Qi Jin:** Methodology, Investigation. **Wen Li:** Visualization, Project administration, Formal analysis. **Yue Li:** Methodology, Investigation. **Yan Zheng:** Methodology, Investigation. **Mei Dong:** Writing – review & editing, Writing – original draft, Project administration, Methodology, Investigation, Funding acquisition, Data curation, Conceptualization. **Yaoyao Bian:** Writing – review & editing, Writing – original draft, Supervision, Methodology, Investigation, Funding acquisition, Formal analysis, Data curation, Conceptualization.

Supporting information

Additional Supporting Information may be found in the online version of this article.

Declaration of competing interest

The authors declare that they have no known competing financial interests or personal relationships that could have appeared to influence the work reported in this paper.

Acknowledgments

This work was supported by the National Natural Science Foundation of China (Nos. 82174394, 82374466, 82104110 **and 81704084**), the Science and Technology Development Fund, Macau SAR (No. 0121/2022/A3, 0127/2023/RIA2), the Faculty Research Grants of Macau University of Science and Technology (No. FRG-22-110-FC), the Natural Science Foundation of Jiangsu Province (Nos. BK20210691, BK20240733, BK20201401, BK20211297), Natural Science Foundation of Nanjing University of Chinese Medicine (No. XPT82104110), the China Postdoctoral Science Foundation (2022M721393), and the 333 High-Level Talents Cultivation Project of Jiangsu Province.

Appendix A. Supplementary data

Supplementary data to this article can be found online at https://doi.org/10.1016/j.mtbio.2025.101637.

Data availability

Data will be made available on request.

References

[1] L.M. Foster Ds, C.D. Marshall, G.S. Gulati, M.S. Chinta, A. Nguyen, A. Salhotra, R. E. Jones, A. Burcham, T. Lerbs, L. Cui, M.E. King, A.L. Titan, R.C. Ransom, A. Manjunath, M.S. Hu, C.P. Blackshear, S. Mascharak, A.L. Moore, J.A. Norton, C. J. Kin, A.A. Shelton, M. Januszyk, G.C. Gurtner, Wernig, Elucidating the fundamental fibrotic processes driving abdominal adhesion formation, Nat. Commun. 11 (2020) 4061.

[2] J. Liao, X. Li, Y. Fan, Prevention strategies of postoperative adhesion in soft tissues by applying biomaterials: based on the mechanisms of occurrence and development of adhesions, Bioact. Mater. 26 (2023) 387–412, https://doi.org/10.1016/j.bioactmat.2023.02.026.

[3] J.M. Smith, S.K. Kapur, A.F. Mericli, D.P. Baumann, C.E. Butler, Parastomal hernia repair, Plast. Aesthetic Res. 9 (2022), https://doi.org/10.20517/2347-9264.2021.48.

[4] S. Gillern, J.I.S. Bleier, Parastomal hernia repair and reinforcement: the role of biologic and synthetic materials, Clin. Colon Rectal Surg. 27 (2014) 162–171, https://doi.org/10.1055/s-0034-1394090.

[5] J.A. David, J.A. Gusenoff, Surgical circumferential contouring: lower body, upper body, and in-between, Plast, Aesthetic Res. 9 (2022), https://doi.org/10.20517/2347-9264.2021.67.

[6] J. Tang, Z. Xiang, M.T. Bernards, S. Chen, Peritoneal adhesions: occurrence, prevention and experimental models, Acta Biomater. 116 (2020) 84–104, https://doi.org/10.1016/j.actbio.2020.08.036.

[7] C. Strik, M.W.J. Stommel, R.P.G. Ten Broek, H. Van Goor, Adhesiolysis in patients undergoing a repeat median laparotomy, Dis. Colon Rectum 58 (2015) 792–798, https://doi.org/10.1097/DCR.0000000000000405.

[8] Y.C. Cheong, S.M. Laird, T.C. Li, J.B. Shelton, W.L. Ledger, I.D. Cooke, Peritoneal healing and adhesion formation/reformation, Hum. Reprod. Update 7 (2001) 556–566, https://doi.org/10.1093/humupd/7.6.556.

[9] M. Toneman, T. Groenveld, P. Krielen, A. Hooker, R. de Wilde, L.A. Torres-de la Roche, A. Di Spiezio Sardo, P. Koninckx, Y. Cheong, A. Nap, H. van Goor, P. Pargmae, R. ten Broek, Risk factors for adhesion-related readmission and abdominal reoperation after gynecological surgery: a nationwide cohort study, J. Clin. Med. 12 (2023) 1–12, https://doi.org/10.3390/jcm12041351.

[10] P. Krielen, M.W.J. Stommel, P. Pargmae, N.D. Bouvy, E.A. Bakkum, H. Ellis, M. C. Parker, E.A. Griffiths, H. van Goor, R.P.G. ten Broek, Adhesion-related readmissions after open and laparoscopic surgery: a retrospective cohort study (SCAR update), Lancet 395 (2020) 33–41, https://doi.org/10.1016/S0140-6736(19)32636-4.

[11] R.P.G. Ten Broek, M.W.J. Stommel, C. Strik, C.J.H.M. Van Laarhoven, F. Keus, H. Van Goor, Benefits and harms of adhesion barriers for abdominal surgery: a systematic review and meta-analysis, Lancet 383 (2014) 48–59, https://doi.org/10.1016/S0140-6736(13)61687-6.

[12] P. Krielen, B.A. van den Beukel, M.W.J. Stommel, H. van Goor, C. Strik, R.P.G. ten Broek, In-hospital costs of an admission for adhesive small bowel obstruction, World J. Emerg. Surg. 11 (2016) 1–8, https://doi.org/10.1186/s13017-016-0109-y.

[13] Y. Wang, H. Zhang, Y. Chen, L. Yang, Z. Li, M. Zhao, W. Li, Y. Bian, L. Zeng, Research on mechanisms of Chinese medicines in prevention and treatment of postoperative adhesion, Chin. J. Integr. Med. 29 (2023) 556–565, https://doi.org/10.1007/s11655-023-3735-0.

[14] J. Zindel, J. Mittner, J. Bayer, S.L. April-Monn, A. Kohler, Y. Nusse, M. Dosch, I. Büchi, D. Sanchez-Taltavull, H. Dawson, M. Gomez de Agüero, K. Asahina, P. Kubes, A.J. Macpherson, D. Stroka, D. Candinas, Intraperitoneal microbial contamination drives post-surgical peritoneal adhesions by mesothelial EGFR-

signaling, Nat. Commun. 12 (2021), https://doi.org/10.1038/s41467-021-27612-x.
[15] X. Xu, A. Rivkind, O. Pappo, A. Pikarsky, F. Levi-Schaffer, Role of mast cells and myofibroblasts in human peritoneal adhesion formation, Ann. Surg. 236 (2002) 593–601, https://doi.org/10.1097/00000658-200211000-00009.
[16] J. Zindel, M. Peiseler, M. Hossain, C. Deppermann, W.Y. Lee, B. Haenni, B. Zuber, J.F. Deniset, B.G.J. Surewaard, D. Candinas, P. Kubes, Primordial GATA6 macrophages function as extravascular platelets in sterile injury, Science 371 (2021), https://doi.org/10.1126/science.abe0595, 0–12.
[17] H.X. Zhidong Lv, Di Na, Xiaoyang Ma, Chong Zhao, Weijun Zhao, Human peritoneal mesothelial cell transformation into myofibroblasts in response to TGF-ß1 in vitro, Int. J. Mol. Med. 27 (2011) 187–193.
[18] L. Yang, Z. Lian, B. Zhang, Z. Li, L. Zeng, W. Li, Y. Bian, Effect of ligustrazine nanoparticles on Th1/Th2 balance by TLR4/MyD88/NF-κB pathway in rats with postoperative peritoneal adhesion, BMC Surg. (2020) 1–8, https://doi.org/10.21203/rs.3.rs-26682/v1.
[19] H. Zhang, Y. Song, Z. Li, T. Zhang, L. Zeng, W. Li, Y. Bian, Evaluation of ligustrazine on the prevention of experimentally induced abdominal adhesions in rats, Int. J. Surg. 21 (2015) 115–121.
[20] H. Zhang, D. Li, Z. Li, Y. Song, Effect of Ligustrazine on rat peritoneal mesothelial cells treated with lipopolysaccharide, Ren. Fail. 38 (2016) 961–969, https://doi.org/10.3109/0886022X.2016.1165053.
[21] J. Wang, C. Dong, Z. Song, W. Zhang, X. He, R. Zhang, C. Guo, C. Zhang, F. Li, C. Wang, C. Yuan, Monocyclic monoterpenes as penetration enhancers of ligustrazine hydrochloride for dermal delivery, Pharmaceut. Dev. Technol. 22 (2017) 571–577, https://doi.org/10.1080/10837450.2016.1189936.
[22] J. Chen, X. Tang, Z. Wang, A. Perez, B. Yao, K. Huang, Y. Zhang, M.W. King, Techniques for navigating postsurgical adhesions: insights into mechanisms and future directions, Bioeng. Transl. Med. 8 (2023), https://doi.org/10.1002/btm2.10565.
[23] V.H. Schmitt, A. Mamilos, C. Schmitt, C.N.E. Neitzer-Planck, T.K. Rajab, D. Hollemann, W. Wagner, B. Krämer, H. Hierlemann, C. James Kirkpatrick, C. Brochhausen, Tissue response to five commercially available peritoneal adhesion barriers—a systematic histological evaluation, J. Biomed. Mater. Res. Part B Appl. Biomater. 106 (2018) 598–609, https://doi.org/10.1002/jbm.b.33835.
[24] J. Cai, J. Guo, S. Wang, Application of polymer hydrogels in the prevention of postoperative adhesion: a review, Gels 9 (2023), https://doi.org/10.3390/gels9020098.
[25] H. Braet, P.P. Fransen, Y. Chen, S. Van Herck, R. Mariën, V. Vanhoorne, W. Ceelen, A. Madder, S. Ballet, R. Hoogenboom, B. De Geest, A. Hoorens, P.Y.W. Dankers, S. C. De Smedt, K. Remaut, Smart hydrogels delivered by high pressure aerosolization can prevent peritoneal adhesions, J. Contr. Release 362 (2023) 138–150, https://doi.org/10.1016/j.jconrel.2023.08.042.
[26] C. Cui, T. Wu, X. Chen, Y. Liu, Y. Li, Z. Xu, C. Fan, W. Liu, A Janus hydrogel wet adhesive for internal tissue repair and anti-postoperative adhesion, Adv. Funct. Mater. 30 (2020) 1–11, https://doi.org/10.1002/adfm.202005689.
[27] X. Peng, X. Xia, X. Xu, X. Yang, B. Yang, P. Zhao, W. Yuan, P.W.Y. Chiu, L. Bian, Ultrafast self-gelling powder mediates robust wet adhesion to promote healing of gastrointestinal perforations, Sci. Adv. 7 (2021) 1–13, https://doi.org/10.1126/sciadv.abe8739.
[28] L. Wang, L. Sun, Z. Gu, W. Li, L. Guo, S. Ma, L. Guo, W. Zhang, B. Han, J. Chang, N-carboxymethyl chitosan/sodium alginate composite hydrogel loading plasmid DNA as a promising gene activated matrix for in-situ burn wound treatment, Bioact. Mater. 15 (2022) 330–342, https://doi.org/10.1016/j.bioactmat.2021.12.012.
[29] J. Yang, M. Shen, Y. Luo, T. Wu, H. Wen, J. Xie, Construction and characterization of Mesona chinensis polysaccharide-chitosan hydrogels, role of chitosan deacetylation degree, Carbohydr. Polym. 257 (2021) 117608, https://doi.org/10.1016/j.carbpol.2020.117608.
[30] M. Naveed, L. Phil, M. Sohail, M. Hasnat, M.M.F.A. Baig, A.U. Ihsan, M. Shumzaid, M.U. Kakar, T. Mehmood Khan, M.D. Akabar, M.I. Hussain, Q.G. Zhou, Chitosan oligosaccharide (COS): an overview, Int. J. Biol. Macromol. 129 (2019) 827–843, https://doi.org/10.1016/j.ijbiomac.2019.01.192.
[31] C. Muanprasat, V. Chatsudthipong, Chitosan oligosaccharide: biological activities and potential therapeutic applications, Pharmacol. Ther. 170 (2017) 80–97, https://doi.org/10.1016/j.pharmthera.2016.10.013.
[32] M. Zhao, Y.Y. Bian, L.L. Yang, Y.Q. Chen, Y.J. Wang, Y.T. Ma, Y.Q. Pei, W.L. Li, L. Zeng, HuoXueTongFu formula alleviates intraperitoneal adhesion by regulating macrophage polarization and the SOCS/JAK2/STAT/PPAR- γ signalling pathway, Mediat. Inflamm. (2019) 2019, https://doi.org/10.1155/2019/1769374.
[33] J. Demuytere, W. Ceelen, J. Van Dorpe, A. Hoorens, The role of the peritoneal microenvironment in the pathogenesis of colorectal peritoneal carcinomatosis, Exp. Mol. Pathol. 115 (2020) 104442, https://doi.org/10.1016/j.yexmp.2020.104442.
[34] J.J. Tomasek, G. Gabbiani, B. Hinz, C. Chaponnier, R.A. Brown, Myofibroblasts and mechano: regulation of connective tissue remodelling, Nat. Rev. Mol. Cell Biol. 3 (2002) 349–363, https://doi.org/10.1038/nrm809.
[35] X.M. Meng, D.J. Nikolic-Paterson, H.Y. Lan, TGF-β: the master regulator of fibrosis, Nat. Rev. Nephrol. 12 (2016) 325–338, https://doi.org/10.1038/nrneph.2016.48.
[36] L. Holmdahl, K. Kotseos, M. Bergström, P. Falk, M.L. Ivarsson, N. Chegini, Overproduction of transforming growth factor-β1 (TGF-β1) is associated with adhesion formation and peritoneal fibrinolytic impairment, Surgery 129 (2001) 626–632, https://doi.org/10.1067/msy.2001.113039.
[37] P. Ten Dijke, C.S. Hill, New insights into TGF-β-Smad signalling, Trends Biochem. Sci. 29 (2004) 265–273, https://doi.org/10.1016/j.tibs.2004.03.008.
[38] Y. Wang, J. Guo, X. Cao, Y. Zhao, Developing conductive hydrogels for biomedical applications, Smart Med 3 (2024) 1–16, https://doi.org/10.1002/smmd.20230023.
[39] Y. Xu, Q. Saiding, X. Zhou, J. Wang, W. Cui, X. Chen, Electrospun fiber-based immune engineering in regenerative medicine, Smart Med 3 (2024), https://doi.org/10.1002/smmd.20230034.